Proceedings of the 9th World Congress on Mechanical, Chemical, and Material Engineering (MCM'23)
Brunel University, London, United Kingdom - August 06-08, 2023
Paper No. ICMIE 132
DOI: 10.11159/icmie23.132

Bending Stress in Worm Gear Shafts Considering The Notch Effect And The Load Distribution

Johannes Gründer[1], Alexander Monz[2]
[1,2]Nuremberg Institute of Technology
Kesslerplatz 12, 90489 Nuremberg, Germany
[1]johannes.gruender@th-nuernberg.de; [2]alexander.monz@th-nuernberg.de

Abstract – Worm gear units are helical gear units with an axis cross angle of 90°. The load distribution on several tooth flanks enables the transmission of high torques. The worm shaft is made of case-hardened steel and the worm wheel of a bronze alloy to avoid scuffing in the tooth contact due to high temperatures in the contact area. Since the wheel is made of a softer material, the gear units usually fail due to damage of the wheel. Common causes of damage are wear, pitting or fracture of a wheel tooth or the entire rim. According to the state of the art, the worm shaft is mostly designed against deflection. In the further literature, cases of tooth breakage of worm shafts are also documented. By modifying the gear geometry or using higher strength materials for the worm wheel, the worm shafts may fail due to force or fatigue fracture under high loads. The accuracy of the gear assembly also has a significant impact on the load distribution of gear units. Deviations in the nominal positions of the components may cause load increases and accelerate the failure of the gear unit. To estimate the influence of the assembly deviations on the bending stress in the worm shaft, this paper presents an analytical calculation approach for determining the bending stress by considering the notch effect, the notch position and the load pattern and distribution. Finally, the bending stresses caused by various load patterns caused by assembly deviations are calculated and the effect is evaluated.

***Keywords*:** Drive Technology, Worm Gears, Strength of Materials, Bending Stress, Simulation

1. Introduction

Worm gear units are helical gear units with an axis cross angle of 90°, high transmission ratios in one gear stage as well as high transmittable torques due to the distribution of the load over several meshing teeth. The worm shaft is made of case-hardened steel and a worm wheel which is usually made of a bronze alloy to avoid scuffing in the tooth contact. The loads applied during operation reduce the service life of the gearbox due to failures of the gear components. The premature failure of the gearbox usually occurs due to damage of the worm wheel such as wear, pitting or fracture of a wheel tooth or the entire rim. Additionally, high temperatures of the lubricant may cause an insufficiently formed lubricant film and may reduce the service life even further.

In the state of the art, the verification of the service life of the worm gear unit is performed mainly for the worm wheel during design according to DIN 3996 [1], ISO/TR 14521 [2], ANSI/AGMA 6022-C93 [3] and BS 721:Part2 [4]. The worm shaft is designed against deflection because excessive displacements may shift the contact pattern, cause load transmission errors, and reduce the service life DIN 3996 [1], [5]. The stiffening effect of the worm shaft geometry was further investigated by [6], an extension by the variable position of the force application is presented in [7]. According to ANSI/AGMA 6022-C93 [3], the worm shaft is additionally designed against fracture of the worm shaft by comparing the nominal bending stress with the tolerable stress of the material used. In [8], the fracture of the worm shaft is also estimated as a necessary component of future design approaches.

Fractures of the worm shaft teeth are documented in [9], [10], [11], [12] and [13] but the design against stress in the tooth root of the worm shaft is not considered within any standardized approach. To calculate the stress in the tooth root, an approach based on the disk theory was presented by [14]. In [15], measurements using optical interferometers were performed from which empirical equations are derived. In [16] an approach based on the Finite Element Method (FEM) is presented and in [17] and [18] the stresses in the worm shaft are evaluated for a specific geometry using the FEM. The damage of the worm tooth flanks caused by grooves were investigated in [19] and [20]. For the calculation of the bending stress of worm shafts no further literature can be found.

2. Bending Stress according to the State of the Art and Load Distribution in Worm Gears

According to ANSI/AGMA 6022-C93 [3], worm shafts are designed against fracture by comparing the nominal bending stress with the tolerable stresses of the used materials. The worm geometry is assumed as a round beam with the diameter corresponding to the root circle diameter d_{f1} of the worm shaft. The tooth forces are applied in axial, radial and tangential direction (F_{xm1}, F_{rm1} and F_{tm1}) acting in a single point at the centre circle diameter d_{m1}. The calculation model according to ANSI/AGMA 6022-C93 [3] and [21] is shown in Fig. 1.

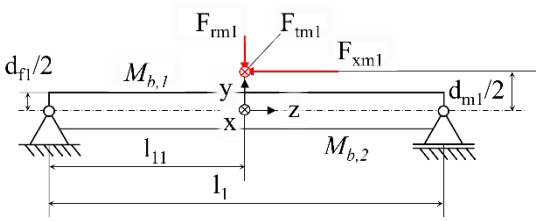

Fig. 1 Model for calculating the bending stress according to ANSI/AGMA 6022-C93 [3] and [21]

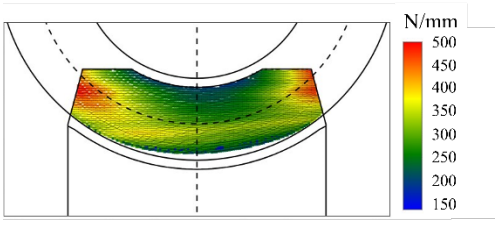

Fig. 2 Example load distribution calculated with SNETRA [22]

The reaction forces of the bearings of the worm shaft are calculated. The bending moment M is determined by cutting reactions in the beam. For this purpose, the first cut in the beam is located between the bearing on the left and the tooth forces, and the second cut is located between the tooth force and the bearing on the right as shown in Fig. 1. For verifying the strength, the maximum bending moment of the bending moments $M_{b,1}$ and $M_{b,2}$ in these segments is used. The nominal bending stress according to ANSI/AGMA 6022-C93 [3] is calculated according to Eq. (1).

$$\sigma = \frac{max\left(M_{b,1}, M_{b,2}\right)}{\frac{\pi}{32} \cdot {d_{f1}}^3} \tag{1}$$

When designing worm gear units beyond the usual standard documents, the load distribution in the tooth contact is calculated to further optimize the design regarding wear, pitting, local temperatures and the lubrication film. Various software solutions (e.g. SNETRA [22] or ZSB [23]) are available for this purpose. Fig. 2 shows an example of the load distribution calculated with SNETRA for the deviation-free standard reference geometry according to DIN 3996 [1] and DIN 3975-1 [24] for the rotational speed of the worm shaft $n_1 = 60$ rpm and the torque $T_2 = 1.350$ Nm acting on the worm wheel. According to ISO/TR 10828 [25], the contact pattern for non-loaded engagement can be calculated.

3. New Analytical Model for Calculating the Bending Stress

The tooth space of worm shafts can be considered as a helical circumferential notch. In mechanical engineering, the maximum local stress occurring in a notched component under load is usually calculated based on a nominal stress approach. In most cases, the geometry and load need to be simplified for an analytical approach because of the complexity of the components. The maximum local stress σ_0 in the notch is then obtained by multiplying the nominal stress σ_{nenn} by factor α_K for considering the stress concentration in the notch. The calculation for a circular notched beam of diameter d and bending resistance W_b loaded with a bending moment M_b is performed according to Eq. (2).

$$\sigma_0 = \sigma_{nenn} \cdot \alpha_K = \frac{M_b}{W_b} \cdot \alpha_K \tag{2}$$

The bending stress distribution of an unnotched circumferential beam and in a double-threaded worm shaft are shown in Fig. 3. The location of the maximum bending stress in the cross section is located on the surface in the centre of the tooth gap at the root circle diameter d_{f1}. The bending stress in the cross-section of the worm shaft is rotated in

2a) - 2d) by the rotation angle φ_1. The maximum tensile and compressive bending stresses occur when the direction of the bending moment and the location of the tooth gap align in 2c).

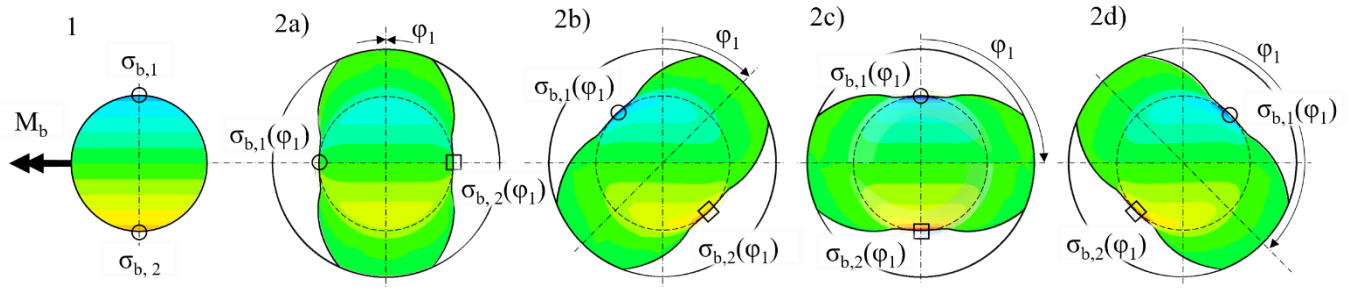

Fig. 3 Bending stress distribution in the cross section of a reference rod (1) and for rotated worm gear shaft cross sections (2a - d)

The dimensionless notch coefficient α_K depends on the geometry of the notch and the type of loading, whereby a distinction is made between tension/compression, bending and torsion. The determination is usually carried out using FEM simulations or analytical approaches (e.g. according to [26]). The notch coefficients of various simple notched shafts can be found in DIN 743-2 [27]. However, helical notches are not treated in the document. The notch effect for the standard worm shaft geometry according to DIN 3996 [1] loaded with a constant bending moment M_b is investigated using FEM simulations. The calculation of the notch coefficient α_K is carried out by comparing the maximum stress $\sigma_{b,max,WS}$ in the tooth gap of the worm shaft to the maximum nominal stress $\sigma_{b,max,nenn}$ of an unnotched round profile loaded with the same bending moment. The notch coefficient is $\alpha_K = \sigma_{b,max,WS} / \sigma_{b,max,nenn} = 2{,}02$. By rotating the cross-section by the angle φ_1, the occurring stress changes depending on the absolute position of the tooth root in relation to the orientation of the bending moment M_b. The periodic bending stresses in the two tooth gaps in the cross section and in the unnotched beam are shown in Fig. 4. The graph of the bending stress is independent of the toothing geometry and mathematically described using the sine function.

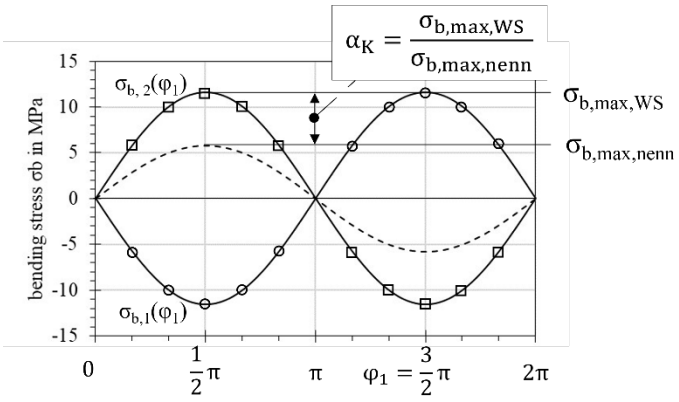

Fig. 4 Stress curve during rotation of the cross section and notch effect

3.1. Bending Stress in Axial Direction and due to Worm Shaft Rotation

According to the calculation approach in ANSI/AMGA 6022-C93 [3], the worm shaft is loaded by the tooth force components acting in a single point at the centre circle diameter in the middle of the shaft. This results in the bending moments M_{xz} and M_{yz} in the respective planes. By considering the changing position of the tooth gap in the cross section along the worm axis due to the helical tooth geometry and the rotation of the worm shaft during operation, the model as shown in Fig. 5 is derived. The coefficient K_p considers the axial and angular position of the observation point and is calculated according to Eq. (3).

$$K_P = \cos\left(\upsilon_{zf,0} + \frac{z}{m_x \cdot z_1 \cdot \pi} \cdot 2\pi + \varphi_1 + \upsilon_{Mb}(\varphi_1, z) + \varphi_n\right) \tag{3}$$

In Eq. (3), the initial angle position of the tooth gap in the reference position is $\upsilon_{zf,0}$, the gears axial modulus m_x, the angle direction of the bending moment in the cross section at the coordinate z is υ_{Mb} and the phase shift of all n tooth gaps in

worm shafts with more than one gear threat is φ_n. Depending on the amount of worm threads z_1, every cross section features n = z_1 notches. The phase shift for every notch in one cross section is calculated according to Eq. (4).

$$\varphi_n = \frac{n-1}{z_1} \cdot 2\pi \tag{4}$$

The axis location and rotation angle dependent bending stress for observation points with different z coordinates under rotation with the angle φ_1 is shown in Fig. 6.

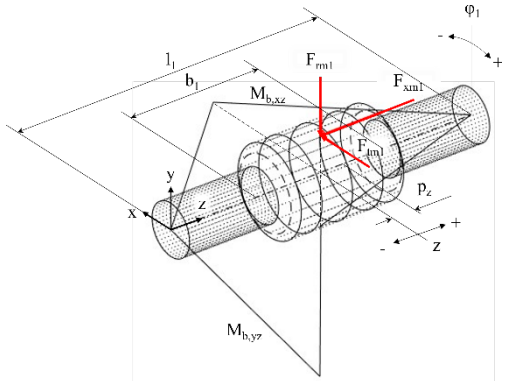

Fig. 5 Bending moment in xz- and yz-plane under point load

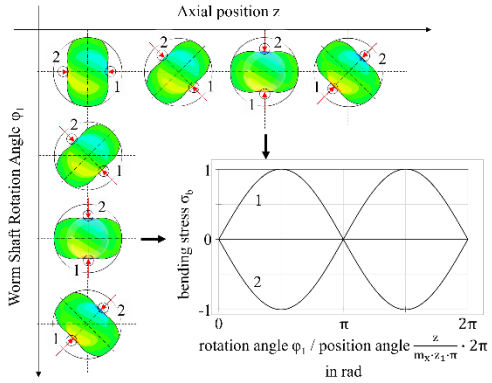

Fig. 6 Bending stress in the worm gear shaft depending on the axial position z and the rotation angle φ_1

The tensile and compressive bending stresses in the tooth gap as a function of the rotation angle φ_1 are shown in Fig. 7 for different thread numbers whereas the position with the maximum tensile stress is displayed in 1a) – d).

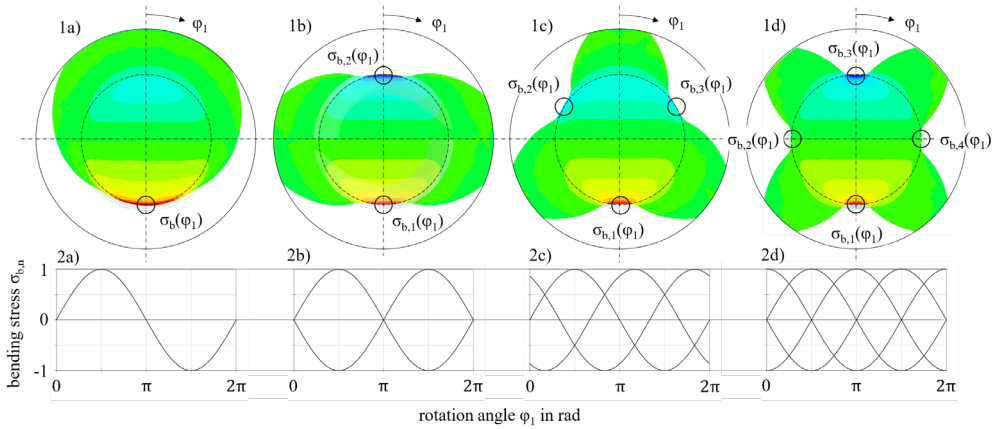

Fig. 7 Angle-dependent bending stress during rotation of the cross section for 1a) $z_1 = 1$, 1b) $z_1 = 2$, 1c) $z_1 = 3$ and 1d) $z_1 = 4$

3.2. Consideration of the Load Distribution in the Tooth Contact

The load distribution in the tooth contact is considered when designing worm gear units beyond the current national or international standards. The calculated load distribution F along a contact line j can be converted into point loads $F_i = (F_{x,i}\ F_{y,i}\ F_{z,i})^T$ at the contact points $P_i = (x_i\ y_i\ z_i)^T$. The force components $F_{x,eji}$, $F_{y,eji}$ and $F_{z,eji}$ are determined by multiplying the total point load F_{eji} by the components $n_{x,i}$, $n_{y,i}$ and $n_{z,i}$ of the normal vector n_i on the worm flank at the contact point P_{eji}. To consider the load distribution when calculating the bending stress, the resulting bending moment $M_{res,e}$ in each engagement position is calculated by summarizing the bending moments M_{eji} resulting from each force

component in each contact point. For this purpose, the approach extended by the variable force application point in [7] based on ANSI/AGMA 6022-C93 [3] is used. The resulting bending moment $M_{res,e}$ is calculated according to Eq. (5).

$$M_{res,e}(\varphi_1, z) = \sum_{j=1}^{m} \sum_{i=1}^{n_{ej}} \sqrt{M_{xz,ji}(z)^2 + M_{yz,ji}(z)^2} \tag{5}$$

The contact lines j of an engagement position e with the load distribution F_{eji} at the contact points P_{eji} are shown as an example in Fig. 8.

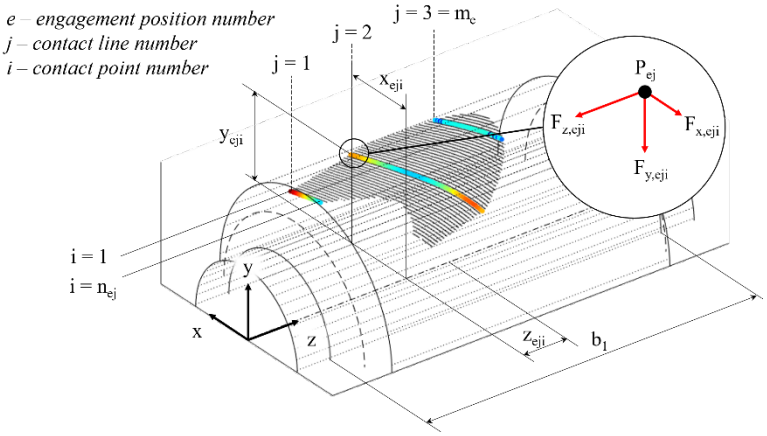

Fig.8 Engagement position e = 1 and simultaneous load distribution on four tooth flanks for a deviation free worm gear as calculated with SNETRA [22]

The contact lines of all other engagement positions of the gears are displayed in black colour. The engagement angle υ_{Mb} of the total bending moment $M_{res,e}$ is calculated for every axial position z using Eq. (6).

$$\upsilon_{Mb}(\varphi_1, z) = \arctan\left(\frac{\sum M_{yz,ji}(\varphi_1, z)}{\sum M_{xz,ji}(\varphi_1, z)}\right) \tag{6}$$

The resulting bending moments for four in the contact pattern equally distributed engagement positions are shown in Fig. 9. The contact lines used for the calculation are shown in Fig. 10.

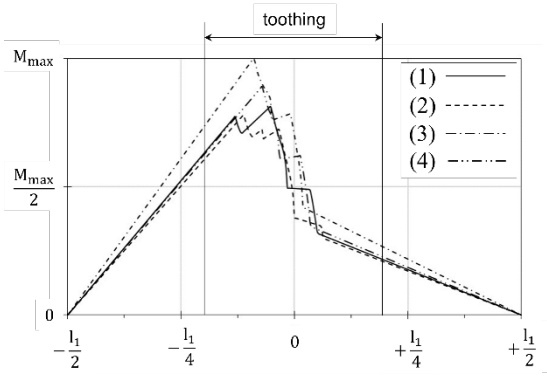

Fig. 9 Bending moment in four engagement positions

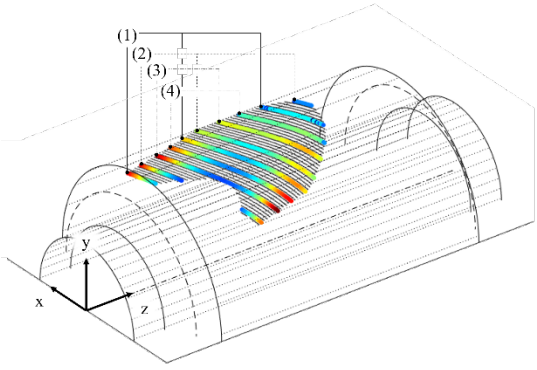

Fig. 10 Load distribution in four engagement positions

3.3. Total Bending Stress in Worm Shafts

The model for considering all previously discussed effects when calculating the bending stress in worm shafts is shown for one cross section at the axial location z in Fig. 11.

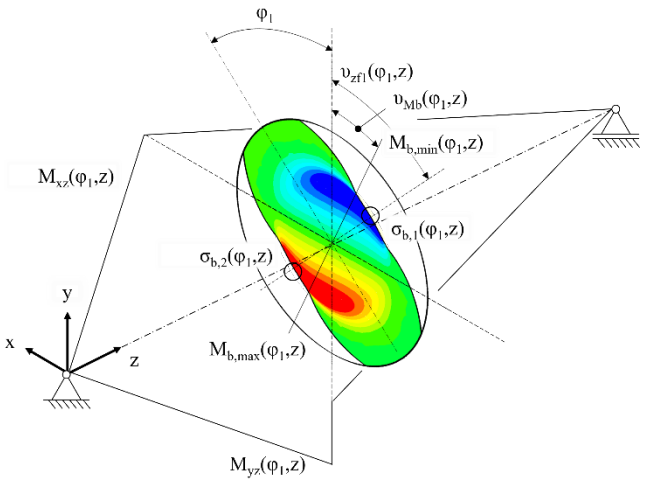

Fig. 11 Model for calculating the bending stress in the entire worm shaft

The bending stress in every engagement position e is calculated using Eq. (2) through (6) according to Eq. (7).

$$\sigma_{b,0} = \frac{\sqrt{M_{xz,ji}(\varphi_1, z)^2 + M_{yz,ji}(\varphi_1, z)^2}}{\frac{\pi \cdot {d_{f1}}^2}{32}} \cdot \cos\left(\upsilon_{zf,0} + \frac{z}{z_1 \cdot m_x \cdot \pi} \cdot 2\pi + \upsilon_{Mb}(\varphi_1, z) + \varphi_1 + \varphi_n\right) \cdot \alpha_K \qquad (7)$$

4. Bending Stress Overload due to Assembly Deviations

Worm gear units are subject to various possible deviations both during manufacture and assembly. For economical production, the permitted deviations must be defined in such a way that the operation of the gear unit is ensured and no premature failures or other disruptive effects occur. The presented approach is used to analyse the influence of the assembly deviations defined in [22] (axial displacement Δa, width displacement Δb, crossing angle error ΔΣ and slope angle error Δβ) for the standard reference gearing according to DIN 3996 [1] and DIN 3975-1 [24]. The load distributions calculated by SNETRA [22] for n_1 = 60 rpm and T_2 = 1.350 Nm are shown in Fig. 12 a) to i) for different assembly deviations. The maximum stress values calculated for the entire contact area are projected in the cross section and displayed in a polar plot. The tensile stresses are displayed in red, the compressive stresses in blue.

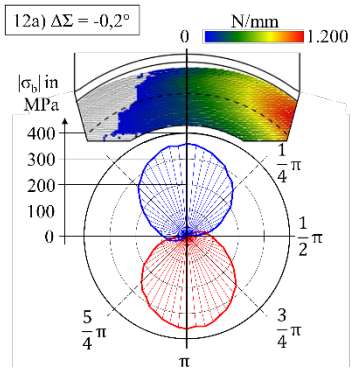

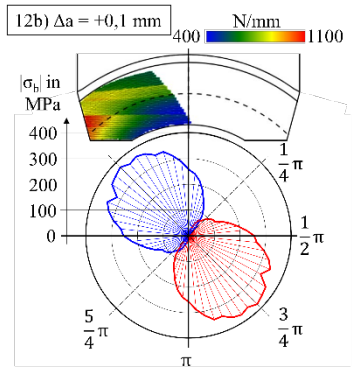

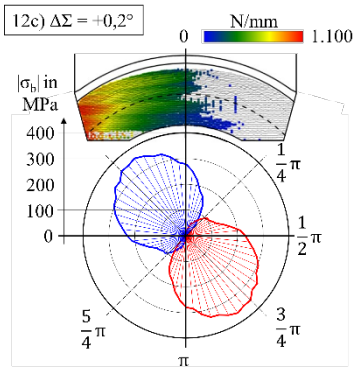

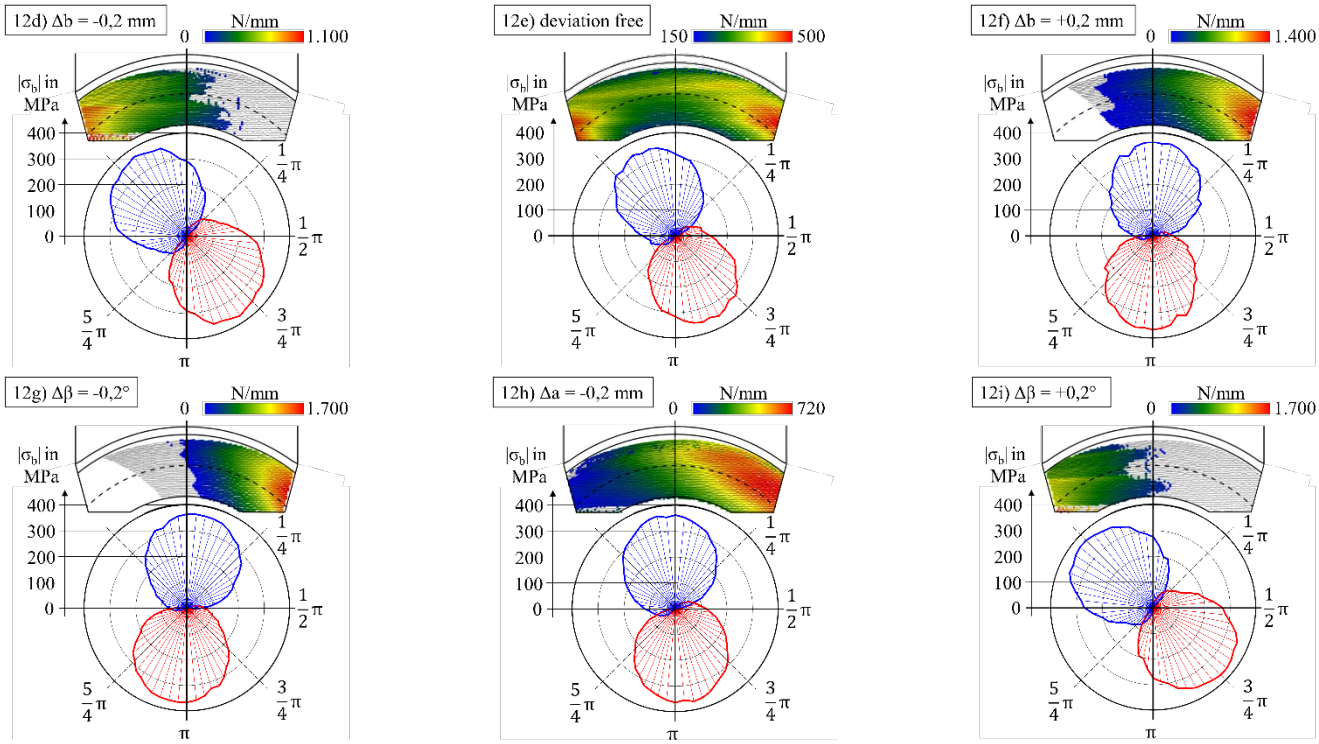

Fig. 12 Load distributions calculated with SNETRA [22] and bending stresses (tensile = red, compressive = blue) for assembly deviations: 12a) negative crossing angle error, 12b) positive axial displacement, 12c) positive crossing angle error, 12d) negative width displacement, 12e) deviation-free, 12f) positive width displacement, 12g) negative slope angle error, 12h) negative axial displacement and 12i) positive slope angle error.

The maximum bending stress according to the approach in ANSI/AGMA 6022-C93 [3] is 261,6 MPa. In comparison, the bending stress for the deviation-free assembly increases by 35 %. The displacement of the contact pattern due to assembly deviations, on the other hand, only slightly increases the material stress but rotates the location of the maximum tensile and compressive stresses. The largest increase of the bending stress occurs due to the positive axial displacement $\Delta a = +0{,}1$ mm by 6% in Fig. 12 b) and the smallest increase due to the negative cross angle error $\Delta\Sigma = -0{,}2°$ by 1% in Fig. 12 a).

5. Conclusion

The presented calculation approach allows the calculation of the bending stresses by considering the notch effect in the tooth gap, the location of the stress maxima and the load distribution. The influence of assembly deviations on the material stress in the worm shaft can be evaluated when designing worm gears, which increases the load capacity of the gearbox by using the remaining resources in the material of the worm shaft. The computational efficiency of the gear may be improved by downsizing the diameters of the worm shafts before reaching the strength limit. Furthermore, the reduction of the worms tooth thickness can increase the wear safety factor of the worm wheel by increasing the wheels tooth thickness without sacrificing the durability of the worm shaft. To enable the calculation of a wide variety of worm shaft geometries, it is necessary to determine the notch effect depending on geometric parameters of the toothing. This may be the subject of further investigations. Worm shafts experience different loads during operation in worm gear units. In addition to the occurring bending stress, the tooth root rounding experiences a combination of bending, compressive and shear stress due to the load transmission in the tooth contact similar to a helical gear. Though, no standardized calculation method is available. The superposition of the bending stress in the cross section and the load in the tooth root form the total stress experienced by worm gear shafts. To perform a material strength check, both load aspects need to be considered. The bearable load of the material needs to be evaluated by performing experimental investigations.

Acknowledgements

This work has been supported by funds of the Nuremberg Institute of Technology.

References

[1] DIN 3996: *Tragfähigkeitsberechnung von Zylinder-Schneckengetrieben mit sich rechtwinklig kreuzenden Achsen*. 2019
[2] ISO/TR 14521: *Gears – Calculation of load capacity of wormgears*. 2009
[3] ANSI/AGMA 6022-C93: *Design Manual for Cylindrical Wormgearing*. 2014
[4] BS 721:Part 2: *Worm Gearing Part 2. Metric units*, 1983
[5] G. Niemann, H. Winter: *Maschinenelemente Band 3*. 2. Auflage. Springer-Verlag Berlin Heidelberg. 1983
[6] P. Norgauer, G. Keinprecht, M. Hein, K. Stahl, "A new approach for the calculation of worm shaft deflection in worm and crossed helical gear drives," AGMA Technical Paper, 2021
[7] J. Gründer, A. Monz, P. Norgauer, "Advanced calculation of the deflection of worm shafts with FEM," in *IOP Conference Series: Materials Science and Engineering* Vol. 1190. 2021
[8] M. Octrue, "Evolution of Worm Gear Standards and their Consequences on Load Capacity Calculation Approach," in *Power Transmission Engineering* September 2014, pp 36-42. 2014
[9] N. Lange, „Hoch fresstragfähige Schneckengetriebe mit Rädern aus Sphäroguss," dissertation, TU München, 2000
[10] R. Thiele, „Zahnfuß-Tragfähigkeitsberechnung für Schneckenräder auf Basis des Zahnfußschädigungskonzeptes," Forschungsvereinigung für Antriebstechnik e.V., FVA-Forschungsheft 784, Frankfurt/Main, 2006
[11] P. Roth, „Verschleiß- und Fresstragfähigkeit von Schneckengetrieben aus höherfesten Werkstoffen bei Langsamlauf für Öl- und Fettschmierung," Forschungsvereinigung für Antriebstechnik e.V., FVA-Forschungsheft 1459, Frankfurt/Main, 2021
[12] M. Geuß, „Tragfähigkeit von Schneckengetrieben beim Einsatz von lebensmittelverträglichen Schmierstoffen mit Kontamination mit Wasser," dissertation RU Bochum, 2013
[13] A. Rhode, E. Wrona, „Induktives Härten von Getriebeschnecken", Forschungsvereinigung für Antriebstechnik e.V., FVA-Forschungsheft 798, Frankfurt/Main, 2006
[14] A. H. Elkholy, A. H. Falah, "Worm Gearing Design Improvement by Considering Varying Mesh Stiffness," in *International Journal of Mechanical and Mechatronics Engineering*, Vol. 9, No.9, 2015
[15] K. Sudoh, Y. Tanaka, S. Matsumoto, Y. Tozaki, "Load Distribution Analysis Method for Cylindrical Worm Gear Teeth," in *Transcriptions of the Japan Society of Mechanical Engineering Series C*, Vol. 59, No. 566, 1995
[16] V. Simon, "Stress analysis in wom gears with ground concave worm profile," in *Mechanism and Machine Theory* Vol. 31, No. 8, pp.1121-1130, 1996
[17] C. Pfister, J- Pfister, L. Kazaz, P. Eberhard, „Stress calculation in worm gears using elastic multibody models," in *The 5th Joint International Conference on Multibody System Dynamics*, Lisboa, Portugal, 2018
[18] F. L. Litvin, I. Gonzalez-Perez, K. Yukishima, A. Fuentes, K- Hayasaka, "Design, simulation of meshing, and contact stresses for an improved worm gear drive," in *Mechanism and Machine Theory* Vol. 42, pp. 940-959, 2007
[19] A. Rhode, "Riefenbildung an einsatzgehärteten Schnecken in Abhängigkeit von Belastung, Drehzahl, Baugröße, Schmierstoff, Tragbildlage und Schneckenradbronze," dissertation RU Bochum, 2011
[20] R. Dinter, "Schneckentragfähigkeitsgrenzen ermitteln und erhöhen," Forschungsvereinigung für Antriebstechnik e.V., FVA-Forschungsheft 518, Frankfurt/Main, 1996
[21] X. Chen, G. Jiang, G. Cheng, "Material Mechanical Performance about Worm Bending and Twisting Deformation for Civil Engineering," *Advanced Materials Research*, vol. 568, pp 187-190. Trans Tech Publications Ltd, Switzerland
[22] M. Lutz, „Methoden zur rechnerischen Ermittlung und Optimierung von Tragbildern an Schneckengetrieben," dissertation, TU München, 2000
[23] W. Predki, „Hertzsche Drücke, Schmierspalthöhen und Wirkungsgrade von Schneckengetrieben," dissertation RU Bochum, 1982
[24] DIN 3975-1: *Begriffe und Bestimmungsgrößen für Zylinder-Schneckengetriebe mit sich rechtwinklig kreuzenden Achsen – Teil 1: Schnecke und Schneckenrad,* 2017
[25] ISO/TR 10828: *Worm gears – Worm profiles and gear mesh geometry,* 2015
[26] H. Neuber, *Kerbspannungslehre – Theorie der Spannungskonzentration, Genaue Berechnung der Festigkeit*. 4. Auflage, Springer-Verlag Berlin Heidelberg, 2001
[27] DIN 743-2: *Tragfähigkeitsberechnung von Wellen und Achsen – Teil 2: Formzahlen und Kerbwirkungszahlen,* 2012